Dynamic Crack-Front Deformations in Cohesive Materials

Thibault Roch,[1] Mathias Lebihain,[2] and Jean-François Molinari[1,*]
[1]Civil Engineering Institute, Materials Science and Engineering Institute, Ecole Polytechnique Fédérale de Lausanne, Station 18, CH-1015 Lausanne, Switzerland
[2]Laboratoire Navier, CNRS (UMR 8205), École des Ponts ParisTech, Université Gustave Eiffel, 6-8 avenue Blaise Pascal, 77455 Marne-la-Vallée, France

(Received 11 June 2022; accepted 25 July 2023; published 31 August 2023)

Crack fronts deform due to heterogeneities, and inspecting these deformations can reveal local variations of material properties, and help predict out-of-plane damage. Current models neglect the influence of a finite dissipation length scale behind the crack tip, called the process zone size. The latter introduces scale effects in the deformation of the crack front, that are mitigated by the dynamics of the crack. We provide and numerically validate a theoretical framework for dynamic crack-front deformations in heterogeneous cohesive materials, a key step toward identifying the effective properties of a microstructure.

DOI: 10.1103/PhysRevLett.131.096101

The propagation of fronts, defining the border between two distinct phases, occurs in numerous physical contexts such as paper wetting [1], combustion [2], polymerization [3], contact mechanics [4], fracture mechanics [5], compressive failure [6], and aseismic slip [7]. Fronts usually roughen due to interaction with heterogeneities. In fracture mechanics, a front marks the spatial separation between intact material and crack, and is thereby called a crack front. It deforms as a consequence of the heterogeneous landscape of toughness, the material resistance to crack propagation. Understanding how these deformations occur allows rationalizing the properties of composite materials [8,9]. In addition, the transition between faceting and microbranching for fast crack propagation is thought to be related to high in-plane curvature of the front [10]. Studying the dynamics of front deformations is thus key to unraveling the complex dynamics of heterogeneous dynamic rupture. Coplanar crack propagation is usually studied using perturbative approaches, such as the first-order model derived by Rice [11] based on the weight functions theory of Bueckner [12]. This approach has then been extended to dynamic rupture [13,14] and also to higher orders [10,15,16]. This framework has been successfully applied to the deformation of crack front for various shapes of defects [16–18] as well as predicting the effective toughness of heterogeneous materials [19–21] and rationalizing the intermittent dynamics of crack-front propagation in disordered media [22]. These models are, however, built on the linear elastic fracture mechanics (LEFM) framework and thereby assume that the dissipation at the crack tip occurs in a finite region, the *process zone*, of negligible size. As a consequence, LEFM-based models are bound to treat each asperity scale indifferently. Yet, elasticity is expected to break down along a finite region at the tip of the crack, and heterogeneities smaller or larger than this length scale are expected to affect the crack dynamics differently [23,24]. Cohesive zone models of fracture [25,26] allow considering a finite dissipation length scale through the introduction of stresses resisting the crack opening near the tip over a finite length, the process zone size. Regarding crack distortion, a recent theoretical study [27] shed light on the importance of considering the process zone size for quasistatic cracks. The presence of a finite dissipation length scale (i) controls the stability of crack fronts and (ii) introduces scale effects in the pinning of crack fronts by heterogeneities of fracture energy, and these effects are strongly dependent on how the toughness variations are achieved. For dynamic rupture, the process zone size is known to shrink with increasing propagation velocity, thus increasing the importance of this length scale relative to the size of the heterogeneities [28–30]. In this Letter, we investigate for the first time the influence of a finite process zone on the deformations of a dynamic crack front. We simulate numerically co-planar cracks loaded under normal tensile stress (mode-I) conditions that propagate through a heterogeneous toughness field. We solve this problem using our open-source implementation [31] of the spectral boundary integral formulation of the elastodynamic equations [32,33] and study the influence of toughness heterogeneities arising from heterogeneities of (i) peak strength and (ii) process zone size. We show that contrarily to LEFM, a finite process zone size introduces scale effects in crack-front deformations, related to the nature of the heterogeneities. We also show that dynamic cracks become more and more oblivious to the nature of heterogeneities and their intensity as their speed approaches the Rayleigh wave speed. The behavior of dynamic crack fronts is comprehensively understood with an analytical model that rationalizes the numerical front deformations.

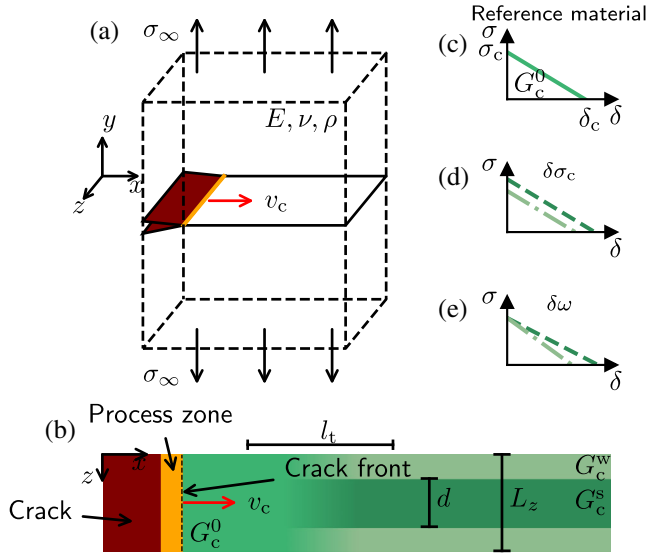

FIG. 1. (a) Two identical semi-infinite elastic bodies are in contact at a planar interface located at $y = 0$, and are loaded under normal tensile stress that drives a crack at a constant velocity v_c. (b) The layout of the interface with the crack (brown), the process zone (orange), and the toughness field (shades of green). The crack front (dashed black line) marks the separation between the process zone and the intact material. (c) Traction-separation law for the reference material. Toughness heterogeneities are achieved by (d) changing the peak strength σ_c or (e) changing the quasistatic process zone size ω_0 but keeping the peak strength constant.

We consider two semi-infinite elastic bodies of section L_x, L_z that are in contact along a planar interface at $y = 0$ [see Fig. 1(a)]. Periodic boundary conditions are imposed in the x and z directions. The bodies are loaded under mode-I condition that drives a cohesive crack through a planar interface [crack in brown, process zone in orange in Fig. 1(b)] in the positive x direction at a constant velocity v_c. The propagation in the $-x$ direction is prevented. The crack initially propagates inside a homogeneous field of reference toughness G_c^0. The interface properties are then gradually changed along a distance l_t towards an x invariant field composed of a stripe of larger toughness G_c^s (dark green) of width d embedded in a weaker toughness field G_c^w (light green). The average toughness in the z direction is kept equal to the reference one, $(G_c^s + G_c^w)/2 = G_c^0$, resulting in an effective toughness in the weak pinning regime (the crack front maintains a stationary shape while propagating) that is equal to G_c^0 [27]. The gradual transition of properties allows reducing the oscillations of the crack-front deformations, see [34]. In this Letter, we use $d = L_z/2$, $L_x = 8L_z$. We study the propagation for only $x < 0.75L_x$ to neglect the effect of periodicity. We employ a linear cohesive law [see Fig. 1(c)] to describe the behavior of the interface, for which the stress decays linearly from a peak value σ_c to 0 with the opening δ up to a critical value δ_c,

$$\sigma^{\mathrm{str}}(x, z, t) = \sigma_c(x, z) \max[1 - \delta(x, z, t)/\delta_c(x, z), 0]. \quad (1)$$

For the linear slip weakening law, the process zone size at rest ω_0 can be estimated as $\omega_0 \simeq 0.731(1 - \nu)\mu\delta_c/\sigma_c$ [36], with ν and μ the Poisson's ratio and the shear modulus of the bulk. The opening is defined as the difference between the displacement fields of the top and bottom solids. In this work, we investigate two types of heterogeneities: (i) heterogeneities of peak strength σ_c with equal process zone size [see Fig. 1(d)] or (ii) heterogeneities of quasistatic process zone size ω_0 with constant peak strength [see Fig. 1(e)]. The toughness contrast is defined as $\Delta G_c = G_c^s - G_c^w$. The problem is solved by conducting full-field dynamic calculations, using an in-house open-source implementation of the spectral boundary integral method [32,33,37] called cRacklet [31]. The details of the method are available in [34]. The crack front is initially perfectly straight and starts deforming when it reaches the heterogeneous field of toughness. The dynamic deformation of the crack front is mediated by the propagation of crack-front waves [29,38,39], resulting in the front oscillating over an equilibrium configuration, see [34]. We measure the amplitude A of the front deformations as the distance between the most advanced point in the process zone at the axis of the strong band and at the axis of the weak band, see Fig. 2(b). We started by validating the ability of our numerical model to capture the linear increase of front deformations amplitude with the toughness contrast, see [34].

First, we investigate the effect of the propagation velocity on the dynamic crack-front deformations. The process zone size at rest ω_0 is kept relatively small compared to the heterogeneities size, and the contrast in toughness is

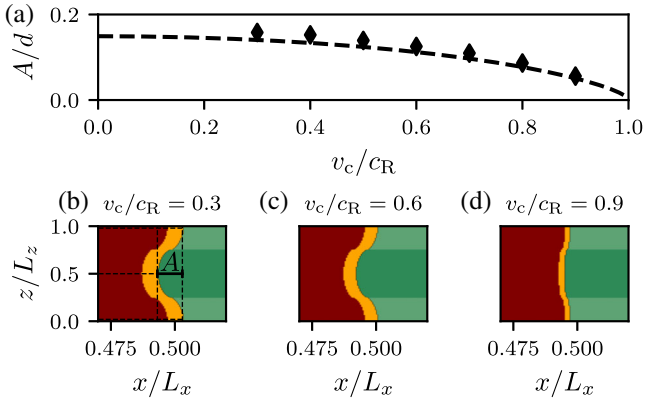

FIG. 2. (a) Normalized amplitude A/d of the front deformations as a function of the normalized propagation velocity v_c/c_R, with the prediction of the classical dynamic line tension model $D_I(v_c)A_{\mathrm{lefm}}/d$ (dashed black), see details in the text. (b)–(d) Snapshots of the interface (with the crack in brown, the process zone in orange, and the intact interface in shades of green corresponding to the toughness) for, respectively, $v_c/c_R = 0.3$, 0.6, 0.9, and $\Delta G_c/G_c^0 = 0.4$. Note that the x scale and z scale are different.

achieved by varying the peak strength while keeping the process zone size at rest constant across the interface. According to [40], a front dynamically stiffens with increasing propagation velocity and thus diminishes its deformations. For fast cracks, more energy is stored as kinetic energy resulting in comparatively lower stored elastic energy and consequently less front deformations. We show in Fig. 2(a) the amplitude A of front deformations as a function of the propagation velocity with $v_c/c_R \in [0.3\text{–}0.9]$ (black diamonds), with c_R the Rayleigh wave speed. The amplitude indeed decreases for faster cracks. The effect of dynamic stiffening on front deformations can be quantified by the function $D_I(v_c)$ which only depends on the propagation velocity and whose derivation is given in [34]. The dashed black line in Fig. 2(a) is $D_I(v_c)A_{\text{lefm}}/d$, with A_{lefm} the predicted amplitude of front deformations based on the classical line tension model which is valid for small process zone size, and this function matches the amplitude observed in the simulations. Figures 2(b)–2(d) are snapshots of the crack-front configuration for $v_c/c_R = 0.3,\ 0.6,\ 0.9$. The crack is shown in brown, the process zone size in orange, and the shades of green stand for the toughness of the intact part of the interface. In these snapshots, two effects of an increasing crack velocity are visible: (i) a decrease in the deformations and (ii) a decrease in the process zone size. The latter is known as the Lorentz contraction [28] of the process zone and is highly relevant for the following when we assess the effect of this length scale on front deformation. The instantaneous process zone size for a mode I crack is given by $\omega_v = \omega_0/A_I(v_c)$ with A_I a universal function of the crack velocity [41].

The influence of the process zone size is investigated. We consider two cases: heterogeneities of peak strength σ_c [with constant process zone, see Fig 1(d)], and heterogeneities of process zone size at rest ω_0 with constant peak strength, see Fig. 1(e). We vary in both cases the average value ω_0 of the quasistatic process zone size while keeping the toughness contrast and the propagation velocity constant. The amplitude of front deformations is shown in Fig. 3(a), for $v_c = 0.5c_R$, $\Delta G_c = 0.4G_c^0$ and $\omega_v/d \in [0.05\text{–}1.5]$ for both heterogeneities of peak strength (diamonds) and process zone size (circles). For small relative process zone size ω_v/d the amplitude is similar for both types of heterogeneities. However, they get significantly farther apart with increasing process zone size: it increases with the dissipation length scale for heterogeneities of peak strength, while it diminishes for heterogeneities of process zone size. Note that this behavior is qualitatively generic and does not depend on the propagation velocity v_c. Changes in process zone size are accommodated more easily by a crack front than changes in peak strength. These observations are striking: the deformations of a cohesive crack propagating through a heterogeneous microstructure are strongly dominated by the nature of the heterogeneities. For two interfaces sharing the same fracture toughness contrast, the difference between the two

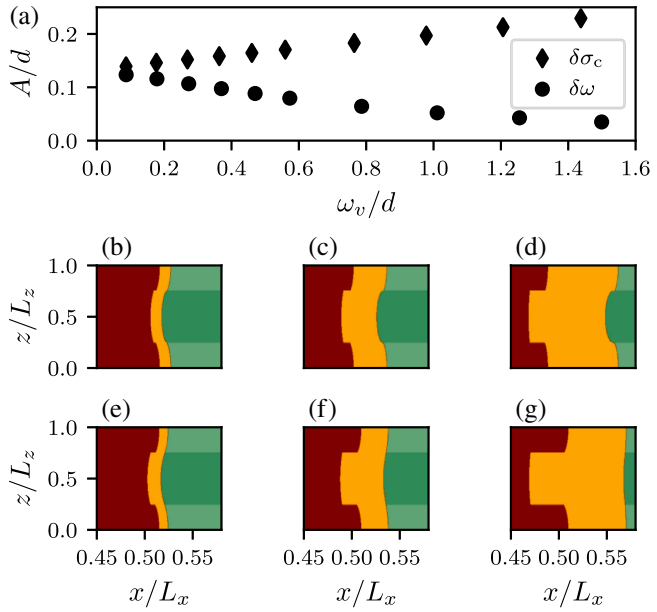

FIG. 3. (a) Scaling of the amplitude A of the front deformations with the process zone size ω_v for heterogeneities of constant process zone size [diamonds, snapshots in (b)–(d) for $\omega_v/d \sim 0.2,\ 0.6,\ 1.25$] and constant peak strength [circles, snapshots in (e)–(g) for $\omega_v/d \sim 0.2,\ 0.6,\ 1.25$]. For the latter, ω_v is the average of $\omega_v(z)$ over the crack front. For these simulations $v_c = 0.5c_R$ and $\Delta G_c/G_c^0 = 0.4$.

types of heterogeneities investigated in this work reaches up to a factor 4 when the process zone and the heterogeneities have the same size $\omega_v/d \sim 1$. The deformations are not tied directly to the toughness contrast, but rather to the variations of the cohesive parameters. For the slip-weakening law used in this Letter and heterogeneities achieved by varying both the peak strength and the process zone size (not presented here), we expect the behavior to be bounded by the two limiting cases that were investigated. This difference vanishes for negligibly small relative process zone size, which can occur either with brittle materials or when cracks propagate at a velocity close to the limiting wave speed due to the Lorentz contraction.

In order to understand these surprising observations, we go back to the *quasistatic cohesive line tension model* that has been recently derived in [27]. Two competing mechanisms arise from the presence of a cohesive zone: (i) the front is *looser* at scales comparable to that of the spatially localized microdamage, (ii) the fluctuations of strength $\delta\sigma_c$ and process zone $\delta\omega$ at that scale are also smoothed out. These competing effects can have two different outcomes in the quasistatic regime [27] that can be understood with the fluctuations of cohesive stress that give rise to a stress intensity factor. The influence of their spatial distribution is controlled by the length scales of the front deformation (d and A). Disorder of strength results in fluctuations concentrated near the tip, so that the front has to distort more to conform to the disordered landscape (increase of A).

For heterogeneities of process zone, the fluctuations occur throughout the entire process zone and especially in its wake, such that the front does not distort much (decrease of A). The overall size of the process zone size ω_v impact the intensity of the cohesive stress fluctuations, thus ruling the potency of these effects on A. This is in qualitative agreement with the results reported in Fig. 3(a). However, our simulations correspond to fully dynamic rupture while the model in [27] is limited to quasistatic cracks. Two additional effects are expected to emerge when extending this model to dynamics: (iii) the process zone size changes dynamically and shrinks when a crack accelerates due to the Lorentz contraction [28] and (iv) the front stiffens with increasing crack velocity [40]. For the same interface, a faster crack is expected to deform less, and the differences between the type of heterogeneities should be reduced. In order to validate our observations, we extend the model of [27] to dynamics in steady state (i.e., constant propagation velocity, see details in [34]) and obtain for the front deformations δa

$$\widehat{\delta a}(k) = -D_I(v_c)\left(\omega_v \frac{\hat{\Sigma}(|k|\omega_v)}{\hat{\mathcal{A}}(|k|\omega_v)} \frac{\widehat{\delta\sigma_c}(k)}{\sigma_c^0} + \omega_v \frac{\hat{\Omega}(|k|\omega_v)}{\hat{\mathcal{A}}(|k|\omega_v)} \frac{\widehat{\delta\omega}(k)}{2\omega_v}\right), \tag{2}$$

with k the wave number, $\hat{\cdot}$ indicating a Fourier transform, ω_v the instantaneous process zone size [related to (iii) above], and $D_I(v_c)$ a function of the velocity that represents the dynamic stiffening of the front [point (iv) above]. $\hat{\mathcal{A}}$, $\hat{\Sigma}$, and $\hat{\Omega}$ are functions of the nature of the weakening, the wave number, and the process zone size (see [34] for their formulation). $\hat{\mathcal{A}}$ acts as (i) the *loss of stiffness* of the front due to the introduction of a finite-size region of dissipation, while $\hat{\Sigma}$ and $\hat{\Omega}$ (ii) smooth out the fluctuations of material properties. In the limit of small ω_v/d, the classical line tension model is recovered.

Crack-front deformation simulations have been conducted for a broad range of parameters, including variations of process zone size at rest ω_0, toughness contrast, heterogeneity type, and front velocity v_c. In Fig. 4(a) the amplitudes measured from the simulations are compared to the predictions from the classical line tension model (i.e., not considering the influence of the process zone size), with the dynamic stiffening term (from Eq. S8 in [34]). This prediction fails, as we have established previously that a finite process zone size strongly impacts the front deformations. For a given prediction based on LEFM (take, for example, $A_{\mathrm{lefm}}/d = 0.25$) there is a large spread of measured amplitude, being either larger or lower than the predicted one (the dashed-gray line has a slope of 1) depending on the heterogeneity type. It is expected from the observations of Fig. 3 that simulations with a small process zone (e.g., for fast ruptures) will result in a significantly smaller difference between the two types of heterogeneities. This is apparent with the data points corresponding to fast cracks [yellow-green in Fig. 4(a)] that are significantly closer than the ones for slower cracks (in blue). The effect of the front stiffening is also visible from Fig. 4(a), with large velocities resulting in small amplitudes. In Fig. 4(b), the prediction of Eq. (2), the newly derived *dynamic cohesive line tension model*, is tested: all the data fall close to a linear master curve, strongly supporting the validity of our model for rationalizing the effect of a finite process zone. While the predictions of Eq. (2) are based on the assumption of a semi-infinite crack, finite-size cracks have been considered in the simulations. Plus, the simulated ruptures are not in a steady state as assumed in the model. Second-order effects might also be required to accurately describe the deformations of cohesive fronts, as the latter can display larger curvatures than the classical line tension fronts. This could potentially explain the small deviations from the predictions. Nonetheless, the proposed model successfully predicts the numerical observations and thereby the nontrivial influence of a finite dissipation length scale for crack-front deformations at constant propagation velocity: not only does the process zone influence front deformations, but also its outcome varies strongly depending on heterogeneity type.

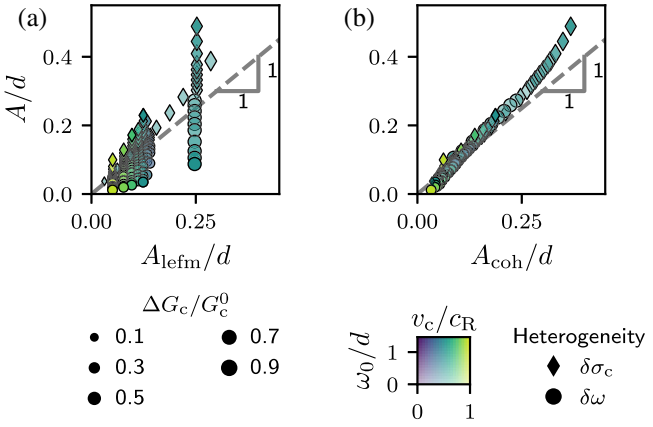

FIG. 4. The front deformations amplitude measured in simulations versus (a) the LEFM prediction not accounting for a finite process zone, (b) the prediction from our newly derived dynamic cohesive line tension model. v_c, ω_0, ΔG_c, and the type of heterogeneities have been systematically varied.

The deformations of a dynamic cohesive crack propagating through a heterogeneous field of toughness have been investigated numerically using the spectral boundary integral method coupled with a cohesive zone model. We show that contrarily to LEFM, a finite process zone size introduces scale effects in the deformation of the crack front that are nontrivial and depend on the nature of the heterogeneities. Fast cracks become more and more oblivious to (i) the nature of the disorder due to the Lorentz contraction of the process zone, and (ii) its intensity due to

the dynamic stiffening of the front. To rationalize these observations, we extended the *cohesive line tension model* recently proposed in [27] to dynamic rupture. This model allows considering heterogeneities at multiple scales, from the nanoscale up to the mesoscale, and predicts accurately the amplitude of the observed deformations, taking into account the instantaneous average process zone size and the propagation velocity. All in all, our model reveals the nontrivial effect of a finite dissipation length scale on the front deformations and particularly the importance of the nature of the heterogeneities. Building a complete cohesive model including changes in velocity and variations of properties along the front propagation direction remains a challenge. For the latter, the process zone size is expected to be also the relevant length scale, as the properties are averaged over the process zone size [23].

We focused here on steady-state crack propagation when material disorder is invariant in the propagation direction. In this limit case, called the weak pinning regime, the energy dissipated in fracture is proportional to the average fracture energy G_c^0. As soon as the translational invariance breaks, crack propagation articulates as the succession of depinning instabilities, and an additional toughening arises from the disorder [42]. The instability threshold is controlled by the energy landscape experienced by the rough crack front. While we do not quantify here the energy balance of dynamic cohesive ruptures, our model provides the necessary ingredients to characterize the impact of the process zone size and heterogeneities on the front roughness, and so on the effective toughness. However, one can already foresee that nearly Rayleigh-wave-speed co-planar cracks with dynamically straightened fronts should propagate in the weak pinning regime. Finally, this work might help understand the occurrence of out-of-plane damage as a consequence of high in-plane curvature of the front [10], and more generally the deformations of a three-dimensional crack front for which the process zone size changes with the orientation from the crack tip.

The scripts used to run the numerical simulations (including the version of the software) and the associated results are available in Ref. [43].

M. Lebihain acknowledges funding provided by the Swiss National Science Foundation (Grant No. CRSK-2_190805).

*jean-francois.molinari@epfl.ch

[1] A. S. Balankin, R. G. Paredes, O. Susarrey, D. Morales, and F. C. Vacio, Phys. Rev. Lett. **96**, 056101 (2006).
[2] J. Maunuksela, M. Myllys, O.-P. Kähkönen, J. Timonen, N. Provatas, M. J. Alava, and T. Ala-Nissila, Phys. Rev. Lett. **79**, 1515 (1997).
[3] E. M. Lloyd, E. C. Feinberg, Y. Gao, S. R. Peterson, B. Soman, J. Hemmer, L. M. Dean, Q. Wu, P. H. Geubelle, N. R. Sottos, and J. S. Moore, ACS Cent. Sci. **7**, 603 (2021).
[4] A. Sanner and L. Pastewka, J. Mech. Phys. Solids **160**, 104781 (2022).
[5] J. Schmittbuhl and K. J. Maloy, Phys. Rev. Lett. **78**, 3888 (1997).
[6] E. Berthier, A. Mayya, and L. Ponson, J. Mech. Phys. Solids **162**, 104826 (2022).
[7] A. Sáez, B. Lecampion, P. Bhattacharya, and R. C. Viesca, J. Mech. Phys. Solids **160**, 104754 (2022).
[8] V. Lazarus, J. Mech. Phys. Solids **59**, 121 (2011).
[9] D. Bonamy and E. Bouchaud, Phys. Rep. **498**, 1 (2011).
[10] I. Kolvin, J. Fineberg, and M. Adda-Bedia, Phys. Rev. Lett. **119**, 215505 (2017).
[11] J. Rice, J. Appl. Mech. **52**, 571 (1985).
[12] H. Bueckner, Int. J. Solids Struct. **23**, 57 (1987).
[13] J. R. Willis and A. B. Movchan, J. Mech. Phys. Solids **43**, 319 (1995).
[14] A. B. Movchan and J. R. Willis, J. Mech. Phys. Solids **43**, 1369 (1995).
[15] J.-B. Leblond, S. Patinet, J. Frelat, and V. Lazarus, Eng. Fract. Mech. **90**, 129 (2012).
[16] M. Vasoya, J.-B. Leblond, and L. Ponson, Int. J. Solids Struct. **50**, 371 (2013).
[17] J. Chopin, A. Prevost, A. Boudaoud, and M. Adda-Bedia, Phys. Rev. Lett. **107**, 144301 (2011).
[18] S. Xia, L. Ponson, G. Ravichandran, and K. Bhattacharya, Phys. Rev. Lett. **108**, 196101 (2012).
[19] S. Patinet, D. Vandembroucq, and S. Roux, Phys. Rev. Lett. **110**, 165507 (2013).
[20] S. M. Xia, L. Ponson, G. Ravichandran, and K. Bhattacharya, J. Mech. Phys. Solids **83**, 88 (2015).
[21] M. Lebihain, Int. J. Fract. **230**, 99 (2021).
[22] J. Barés, A. Dubois, L. Hattali, D. Dalmas, and D. Bonamy, Nat. Commun. **9**, 1253 (2018).
[23] F. Barras, P. H. Geubelle, and J.-F. Molinari, Phys. Rev. Lett. **119**, 144101 (2017).
[24] D. S. Kammer, D. Pino Muñoz, and J. F. Molinari, J. Mech. Phys. Solids **88**, 23 (2016).
[25] D. S. Dugdale, J. Mech. Phys. Solids **8**, 100 (1960).
[26] G. I. Barenblatt, in *Advances in Applied Mechanics*, edited by H. L. Dryden, T. von Kármán, G. Kuerti, F. H. van den Dungen, and L. Howarth (Elsevier, New York, 1962), Vol. 7, pp. 55–129.
[27] M. Lebihain, T. Roch, and J.-F. Molinari, J. Mech. Phys. Solids **168**, 105025 (2022).
[28] J. R. Rice, in *Physics of the Earth's Interior*, edited by A. M. Dziewonski and E. Boschi (North Holland, 1980), pp. 555–649.
[29] J. W. Morrissey and J. R. Rice, J. Mech. Phys. Solids **46**, 467 (1998).
[30] I. Svetlizky and J. Fineberg, Nature (London) **509**, 205 (2014).
[31] T. Roch, F. Barras, P. H. Geubelle, and J.-F. Molinari, J. Open Source Software **7**, 3724 (2022).
[32] P. H. Geubelle and J. R. Rice, J. Mech. Phys. Solids **43**, 1791 (1995).

[33] M. S. Breitenfeld and P. H. Geubelle, Int. J. Fract. **93**, 13 (1998).
[34] See Supplemental Material at http://link.aps.org/supplemental/10.1103/PhysRevLett.131.096101 for additional details on the material properties, the numerical scheme, the identification of the equilibrium amplitude in the simulations and the derivation of the dynamic cohesive line tension model, which includes Ref. [35].
[35] S. Ramanathan and D. S. Fisher, Phys. Rev. Lett. **79**, 877 (1997).
[36] R. C. Viesca and D. I. Garagash, J. Mech. Phys. Solids **113**, 13 (2018).
[37] J. W. Morrissey and P. H. Geubelle, Int. J. Numer. Methods Eng. **40**, 1181 (1997).
[38] F. Fekak, F. Barras, A. Dubois, D. Spielmann, D. Bonamy, P. H. Geubelle, and J. F. Molinari, J. Mech. Phys. Solids **135**, 103806 (2020).
[39] A. Dubois and D. Bonamy, Phys. Rev. E **103**, 013004 (2021).
[40] J. W. Morrissey and J. R. Rice, J. Mech. Phys. Solids **48**, 1229 (2000).
[41] L. B. Freund, *Dynamic Fracture Mechanics* (Cambridge University Press, Cambridge, England, 1998).
[42] V. Démery, A. Rosso, and L. Ponson, Europhys. Lett. **105**, 34003 (2014).
[43] T. Roch, M. Lebihain, and J. F. Molinari, cRacklet simulations for "Dynamic crack front deformations in cohesive materials" (2023), 10.5281/zenodo.7859439.